Atomic Force Microscopy

L. Chaurette, N. Cheng, and B. Stuart

(Dated: November 26, 2016)

Atomic force microscopy is, in many ways, similar to tunneling microscopy and may even be modified to simultaneously measure tunneling. However, the relevant interactions for similar measurements between the two setups often differ. Unlike in tunneling microscopy, atomic force microscopy measures both short and long-range interactions. These forces are often quantified as short-range chemical forces and long-range Van der Waals and electrostatic forces. Operable in static and dynamic modes, destructive and non-destructive methods, and both ultra-high vacuum and aqueous environments, atomic force microscopy is suited to various problems including imaging of biological samples, topography, material characterization, force spectroscopy, atomic resolution and even spin-resolution.

I Introduction

Invented in 1986 by Binnig[1], atomic force microscopy (AFM) was designed as a way to probe material surfaces without the requirement of conducting samples. While atomic force microscopy is, in many ways, similar to tunneling microscopy and may even be modified to simultaneously measure tunneling, the relevant interactions for similar measurements between the two setups, may in fact differ. Unlike in tunneling microscopy, where short-range forces dominate, atomic force microscopy measures both short and long-range interactions. These forces are often quantified as short-range chemical forces and long-range Van der Waals and electrostatic forces, though specific setups may also include additional terms for magnetic forces, or meniscus forces in aqueous environments.[2] To measure these forces, instead of a tunneling tip, the atomic force microscope has a force sensitive cantilever and tip, which measures the tip-sample force $F_{ts} = -\frac{\partial V}{\partial z}$ by means of a tip-sample 'spring constant', $k_{ts} = -\frac{\partial F_{ts}}{\partial z}$. Depending on the operational mode, the force may be measured directly, or otherwise derived from other mode-specific parameters.

While early atomic force microscopy held the tip in contact with the surface, which proved to be a destructive means of characterization, modern AFM is most often operated in a non-contact mode. In addition to the contact mode, the AFM may also be operated in either a static mode, where the cantilever and tip are held in equilibrium, or a dynamic mode, where the tip acts as a forced oscillator, driven by an alternating potential. In dynamic mode, the amplitude is either used as feedback and modulated to a fixed value (Amplitude Modulation, or tapping mode), or the frequency is modulated to resonance (Frequency Modulation). The latter provides the best resolution for atomic imaging, while the former is better suited for aqueous environments and measurements of biological samples.

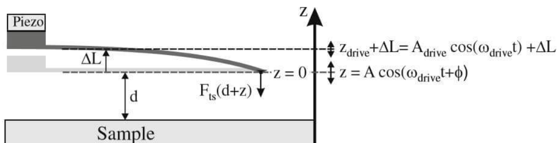

Figure 1. Sketch of the cantilever displacement[3].

II Theory

Static AFM

In the static mode, the sample is probed in the x-y directions with the tip-sample distance kept so small that the cantilever can measure the tip-sample force F_{ts} directly. F_{ts} is given by the derivative of the electrostatic potential between the tip and the sample $F_{ts} = \frac{\partial V_{ts}}{\partial z}$ and is counterbalanced by the deflection of the cantilever

$$F_{tot} = 0 = F_{ts} + F_{cant}, \tag{1}$$

where the cantilever force follows Hooke's law $F_{cant} = -k\Delta z$ with associated natural frequency $f_0 = \frac{1}{2\pi}\sqrt{\frac{k}{m}}$. The most common mode of operation in static AFM is found by keeping the force F_{ts} constant while adjusting the displacement Δz. A topographic image is then acquired by plotting the relative displacement Δz. The forces that make up F_{ts} are, again, a mixture of long-range van der Waals (vdW) and electrostatic forces and short-range repulsive chemical forces. Considering that the long-range interactions are dispersed over many atoms, one may expect atomic resolution to be beyond the reach of static AFM. However, because the tip is kept, during operation, at arbitrarily short distancse from the sample, long-range forces tend to vary much more slowly in comparison with short-range interactions and may be treated roughly as a continuous background. For static AFM, the Lennard-Jones potential,

$$V_{Lennard-Jones}(z) = \epsilon\left[\left(\frac{\sigma}{z}\right)^{12} - 2\left(\frac{\sigma}{z}\right)^{6}\right]. \tag{2}$$

with well depth ϵ and zero-potentail distance σ, is often a good approximation for the short-range chemical interactions, however there are two stable distances z for a given force $F_{Lennard-Jones}$. This may result in measurement errors if the true potential also gives rise to such features and the tip were to jumps from one branch to the other. In practice, static AFM does not achieve atomic resolution due to the mesoscopic properties of the tip, which induce a contact zone dispersed over many atoms as opposed to a single atom.

Dynamic AFM

In dynamic AFM the cantilever is driven by a periodic force with amplitude A_{drive} and frequency f_{drive}. Dynamic AFM is further subdivided into two modes, Amplitude Modulation (AM) and Frequency Modulation (FM).

Amplitude Modulation

AM-AFM detection measures directly the amplitude, A, of the cantilever and the phase ϕ between the cantilever oscillations and the drive force, while keeping A_{drive} and f_{drive} fixed. The measured amplitude is then used as a feedback signal to modulate the equilibrium height, d and driving parameters. It is accurate to model the cantilever as a driven damped harmonic oscillator with the addition of a time-independent tip-sample force F_{ts}. The amplitude of oscillation is assumed to be small in which case the change of F_{ts} is also expected to be small on the order of each oscillation. Therefore, it is often approximated by a linear expansion,

$$F_{ts}(d+z) = F_{ts}(d) + \frac{\partial F_{ts}}{\partial z} z, \tag{3}$$

where d is the equilibrium position of the tip. Now that the force varies linearly with distance, it may be viewed as a spring of constant

$$k' = -\frac{\partial F_{ts}}{\partial z}. \tag{4}$$

The effect of this new spring constant k' is to induce an effective spring constant $k_{eff} = k + k'$, where k is the cantilever spring constant. We always work in the limit $k' \ll k$, where we can approximate the natural frequency to be,

$$\omega_0' = \sqrt{\frac{k+k'}{m}} \simeq \omega_0 \left(1 + \frac{k'}{2k}\right). \tag{5}$$

The new equations of motion for the relative-position z are then,

$$\ddot{z} + \sqrt{\frac{k_{eff}}{m}} \frac{1}{Q} \dot{z} + \frac{k_{eff}}{m} \left(z - z_{drive}\right) = 0, \tag{6}$$

where $z_{drive} = A_{drive} \cos\left(\omega_{drive} t\right)$, is the driven oscillation. Equation (6) corresponds to driven damped harmonic oscillator with dampening inversely proportional to the quality factor Q, generally arising from the effects of the medium in which the sample and tip are immersed. The most general solution to (6) is given by

$$z(t) = A \cos\left(\omega_{drive} t + \phi'\right) + z_{hom}(t), \tag{7}$$

where the first term is the late time solution oscillating at frequency ω_{drive} and z_{hom} is the decreasing exponential solution of the homogeneous differential equation

$$z_{hom}(t) = G e^{-\omega_0' t/2Q} \cos\left(\omega_{hom}' + \phi\right), \tag{8}$$

with $\omega_{hom} = \omega_0' \sqrt{1 - \frac{1}{4Q^2}}$. In AM mode, the user oserves directly the amplitude A which can be related to the tip-sample force via

$$A^2 = \frac{A_{drive}^2}{\left(1 - \frac{\omega_{drive}^2}{\omega_0'^2}\right)^2 + \frac{1}{Q} \frac{\omega_{drive}^2}{\omega_0'^2}} \tag{9}$$

by replacing ω_0' using equations (4), (5).

One of the limits of AM-AFM comes when the quality factor Q is high, which is usually the case in vaccuum where there is little air resistance. In this limit, it takes a characteristic time $\tau \simeq \frac{2Q}{\omega_0'}$ for the homogeneous part of the solution (8) to decay and the system to stabilize to its steady state solution. For large values of the quality factor Q and reasonable values of ω_0', this characteristic time can be as large as $\tau > 10$ms, which is too long to feasibly scan a full sample. In this case, AM-AFM fails and one has to resort to Frequency Modulation (FM) scanning.

Frequency Modulation

In FM-AFM, the cantilever does not oscillate at constant ω_{drive}. Instead, the frequency is modulated to always be at resonance. At resonance, the amplitudes of oscillation are large and the force can no longer be expected to vary linearly. The new equations of motion for the cantilever tip are,

$$m\ddot{z} + \frac{m\omega}{Q} \dot{z} + k\left(z - z_{drive} - \Delta L\right) = F_{ts}(d+z), \tag{10}$$

where the term ΔL corresponds to the static cantilever bending force at $z = 0$. At resonance, the phase difference between the driving force and the position of the cantilever is $\phi = -\frac{\pi}{2}$. The position of the cantilever tip therefore takes the form $z(t) = A \sin \omega t$. Multiplying eq (10) by $A \sin \omega t$ and integrating over a period of oscillation, we get

$$(k - m\omega^2) A^2 \int_0^T dt \sin^2 \omega t = A \int_0^T dt F_{ts}(d + z(t)) \sin \omega t, \tag{11}$$

where the terms proportional to $\sin \omega t$ and $\sin \omega t \cos \omega t$ vanish when integrated over an oscillation period. As the tip-sample force is a small pertubation compared to the driving force, we expect the correction to the resonance amplitude to be small, $\omega \simeq \omega_0 + \Delta\omega$. Dividing by the mass, to first order, the multiplier on the left-hand side of (11) is $(\omega_0 - \omega)(\omega_0 + \omega) \simeq -2\omega_0 \Delta\omega$. In terms of the normal frequency shift,

$$\Delta f = -\frac{1}{4\pi^2 m A f_0} \int_0^T dt F_{ts}(d + A \sin \omega t) \sin \omega t. \tag{12}$$

The right-hand side can be recognized as the time average over a period of the product between F_{ts} and z, leading to

$$\frac{\Delta f}{f_0} = -\frac{1}{A^2 k} \langle F_{ts} \cdot z \rangle_T. \tag{13}$$

Finally, by a change of variable $t \to z(t)$ in the integral, a position dependent integral can be formualted. After some algebra,

$$\frac{\Delta f}{f_0} = -\frac{1}{\pi A^2 k} \int_{-A}^{A} dz \, F_{ts}(d+z) \frac{z}{\sqrt{A^2 - z^2}}. \tag{14}$$

Because the denominator goes to zero as $z \to A$, one expects largest contributions to the frequency shift to be at the points of closest and furthest appraoch. While inverting equation (14) to get the force $F_{ts}(d)$ is generally hard, the fact that the main contributions come from the points $F_{ts}(d \pm A)$ allows one to approximate the force to high precision.

Interactions

To quantify the various interactions present during the measurement, to first order, one often characterizes the frequency shift as roughly a sum of frequency shifts $\Delta f \approx \Delta f_v + \Delta f_{vdW} + \Delta f_{chem}$ from the various contributing interactions, which are also assumed to be additive. These forces generally will depend on the geometry of the sample and the AFM tip. For simplicity, one can assume an infinte flat surface and a mesoscopic cone tip with a spherical cap and a microscopic tip[4] (see Fig. 2a). The distinguishment between the mescoscopic and microscopic portions will be important when considering long and short range interactions. In this geometry, these forces have been approximated by Guggisberg et al. The electrostatic force is,

$$F_v = -\pi\epsilon_0(V_s - V_c)^2 \left[\frac{R}{\bar{s}} + k\alpha^2 \left(\ln\frac{L}{\bar{s}+R_\alpha} - 1\right) - \frac{R[1-k(\alpha)^2\cos^2\alpha/\sin\alpha]}{\bar{s}+R_\alpha]}\right], \tag{15}$$

with 2α the angle between the edges of the cone, $\bar{s}$, the distance of closest approach to the mesoscopic tip, $L \gg \bar{s}$, the tip length, $R_\alpha = R(1-\sin\alpha)$ the radius of the half-sphere, spherical cap, $k(\alpha) = 1/\ln[\cot(\alpha/2)]$ and V_s and V_c are the applied voltage and surface potential respectively. The van der Waals force is then,

$$F_{vdW} = -\frac{H}{6}\left[\frac{R}{\bar{s}} + \frac{\tan^2\alpha}{\bar{s}+R_\alpha} - \frac{R_\alpha}{\bar{s}(\bar{s}+R_\alpha)}\right], \tag{16}$$

where H is the average Hamaker constant for the van der Waals force of the tip and sample. Lastly, the chemical force is approximated by a Morse potential for the bonding,

$$F_{chem} = \frac{2U_0}{\lambda}\left[\exp\left(-2\frac{s-s_0}{\lambda}\right) - \exp\left(-\frac{s-s_0}{\lambda}\right)\right] \tag{17}$$

where s_0 is the minimum of the Morse interaction potential, U_0 is the bonding energy and λ is the characteristic length-scale of the interaction. Note, s is used to denote the position of closest approach to the microscopic tip, as the expected order of λ is less than 1 Å.

Advantageously, these forces are relevent on varying length scales, as illustrated in Fig. 2b. Therefore, a powerful quantitative method is, beginning with large separation distances, to measure the long-range electrostatic and then mid-range van der Waals forces, before gradually moving to smaller separation distances to measure the chemical force.

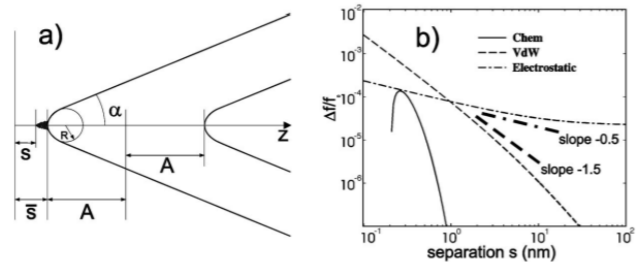

Figure 2. a) Tip and sample geomtry: s is the microscopic distance to the tip, $\bar{s}$ is the mescoscopic distance to the tip, A is the oscillation amplitude, α is the half-angle of the conical tip and R is the radius of the spherical cap. b) Log-log plot of the frequency shifts of the individual interactions for typical experimental values. Image adapted from Guggisberg et al.[4]

III Experimental Methods

Topography

Many researchers require atomically flat surfaces and use AFM to characterize the properties of their materials prior to further work (such as material growth). For this type of work, AFM analysis is often done in air and at room temperature using a device such as Asylum Research's Cypher AFM[5]. These devices often operate in contact mode which has poor lateral image resolution, but provides enough information on surface roughness, while also allowing for quick and simple sample transfers.

Atomic Resolution Imaging

One of the most widely used applications of AFM is its ability to image material surfaces at the sub-Angstrom level. Instead of operating in a contact mode, where frictional forces and the finite radius of the tip can often result in distorted or blurred images, the AFM is operated in the frequency modulated non-contact mode. Introducing multiple vibration damping stages and lowering the temperature into the range of 4K when atoms and molecules are less mobile and electronic noise is minimized, also improves resolution. Atomic resolution images can be seen by F. J. Giessibl[6] in 1995 on Si(111), with its unique 7x7 crystal lattice (Fig. 3A).

Modern advances in the geometry of the tip have greatly increased the resolution one can achieve through AFM as can be seen in the images produced by Katherine Cochrane at the UBC Laboratory for Atomic Imaging Research (LAIR). This image in Fig. 3B was taken with a modern Omicron AFM using a tungsten tip by maintaining a constant frequency shift by adjusting the z-height. As it has been shown that small distances improve resolution, modern AFM imaging is operated in the small tip-sample distance limit, where chemical interactions are maximized. At these small distances, a cantilever with a high stiffness was beneficial, allowing the amplitude to be small[7].

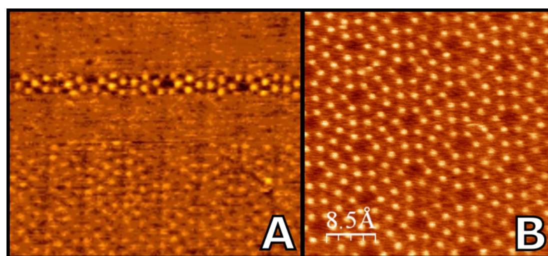

Figure 3. **(A)** The first AFM image of Si(111) with 7x7 reconstruction as taken by Giessibl[6] in 1995. **(B)** Modern AFM image of Si(111) with 7x7 reconstruction taken by K. Cochrane in 2012 (UBC LAIR) showing the incredible progression in image resolution.

Imaging Organic Molecules

As outlined by Bertels et. al[8], placing the AFM tip over an organic molecule, in this case CO, and applying a strong bias voltage can cause the molecule to hop from the surface of the sample to the tip, where it remains attached. This results in a 'new' CO terminated tip with a well defined tip apex which is ideal for imaging in the region where chemical forces are dominant. One of the most famous papers outlining this effect is from L. Gross et al[9], where, for the first time, the individual atoms within an organic molecule (Pentacene, $C_{22}H_{14}$) can clearly be seen (Fig 4). In these experiments, the tip was held at a constant height, z, and the frequency shift of the cantilever was measured. From the measured frequency shift, the vertical force can be extracted and a height profile rendered. Due to pentacene's semiconducting nature, the STM image in Fig. 4B does not produce the same sharp characteristics seen in the AFM image of Fig. 4C.

Chemical Identification of Surface Atoms

In scanning probe microscopy, often the identity of surface atoms is unknown. This can arise from different cleavage planes or impurities that stick to the surface. AFM can be employed as a method of chracterization to determine the chemical composition of such surfaces[10–12]. This has been demonstrated by Y. Sugimoto et al. in a 2007 paper titled "Chemical identification of individual surface atoms by atomic force microscopy"[13]. In their experiment, tin (Sn), lead (Pb) and silicon (Si) were randomly deposited onto a surface of an Si(111) substrate. These three materials exhibit nearly identical chemical and electrical properties, making them indistinguishable via STM, but also have identical preferences for their locations atop of the lattice of Si(111), which further complicates imaging via AFM topography. In Fig. 5A, a topographic image of the surface after Pb, Sn, and Si were deposited atop Si(111) was taken. While there is a clear topography, the atomic identities are indistinguishable in this image. Referring to Fig. 5B, the overlap in topographic height between Pb and Sn atoms shows just how impossible it is to determine chemical composition from a standard topographical map. To distinguish the atoms, Sugimoto et al. instead characterized the maximum attractive force via force spectroscopy and compared the relative

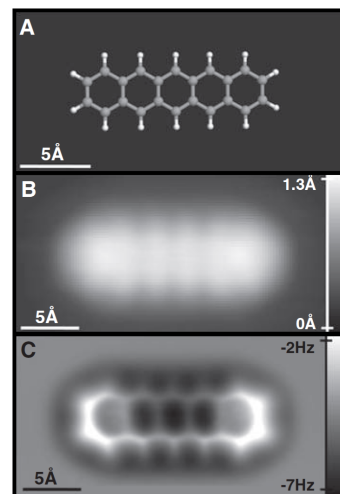

Figure 4. **(A)** A simple ball and stick model of Pentacene ($C_{22}H_{14}$). **(B)** STM image done with constant current settings. **(C)** Constant height AFM with CO terminated tip measuring frequency shift. All images obtained from L. Gross et al. paper[9].

interaction ratios of Pb and Sn to Si (see Fig. 5 C and D). Making force spectroscopy maps of each individual atom (see Fig. 5F), they showed that three distinct bumps occur, corresponding to the maximum attractive forces found in Fig. 5 C and D. Fig. 5E nicely visualizes this data, with an alternating colour scheme for different types of atoms.

Magnetic Exchange Force Microscopy

Many materials exhibit magnetic properties and in order to fully characterize these phenomena, a spatially resolved measurement of the spin properties is valuable. As outlined in S. Heinze's 2000 paper, this can be accomplished with spin polarized STM, however, only on conducting samples[14]. In contrast spin polarized AFM, which utilizes a spin polarized tip, is possible to image magnetic properties of even insulating materials. This was demonstrated by U. Kaiser et al. on a measurement of antiferromagnetic nickel oxide (NiO) using an iron coated silicon tip, with spin polarized perpendicular to the surface of the material by a 5T magnetic field (see Fig. 6)[15].

Their results (Fig. 7) showed standard AFM scans in (A), while the tip was held at a constant resonant frequency shift of $\Delta f = -22$ Hz for an initial distance. With the tip too far from the sample, spin-spin interactions don't play a crucial role in the measured forces. Both the Nickel atoms with spins parallel and anti-parallel to the tip's spin show up as being the same height. However, (B) was taken at a frequency shift of $\Delta f = -23.4$ Hz, causing the tip to move approximately 30 pm closer to the sample. This increased the spin-spin interaction between tip and sample causing an attraction between parallel spins to the tip and a repulsive interaction between anti-parallel spins. The parallel spins, thus appear qualitatively higher on the surface compared with the anti-parallel spins, which appear to recede into the surface. This can be clearly seen in every second diagonal row of Nickel atoms (Fig. 7B), where the topographic height is higher than it's neighboring Nickel atoms.

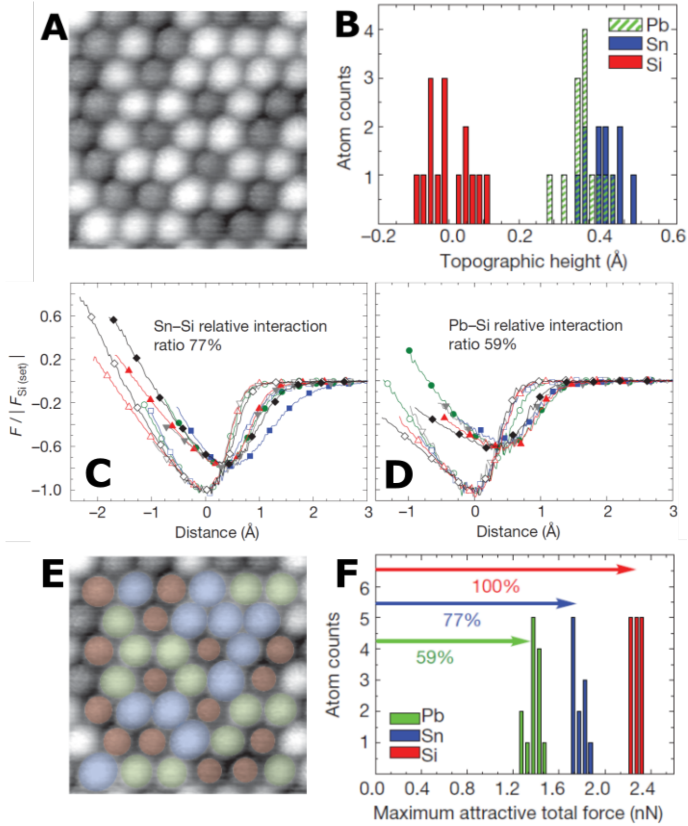

Figure 5. **(A)** AFM image of surface after random deposition of Si, Sn, and Pb. **(B)** Topographic histogram of atoms in (A). **(C)** Relative interaction measurements between tin and silicon normalized to the maximum force of silicon. At maximum attractive force, the interaction ratio is 77%. **(D)** Relative interaction measurements between lead and silicon normalized to the maximum force of silicon. At maximum attractive force, the interaction ratio is 59%. **(E)** Colourized version of (A) distinguishing between atom types. **(F)** Maximum attractive force histogram of (A) obtained via force spectroscopy. All images adapted from Y. Sugimoto et al. paper[13].

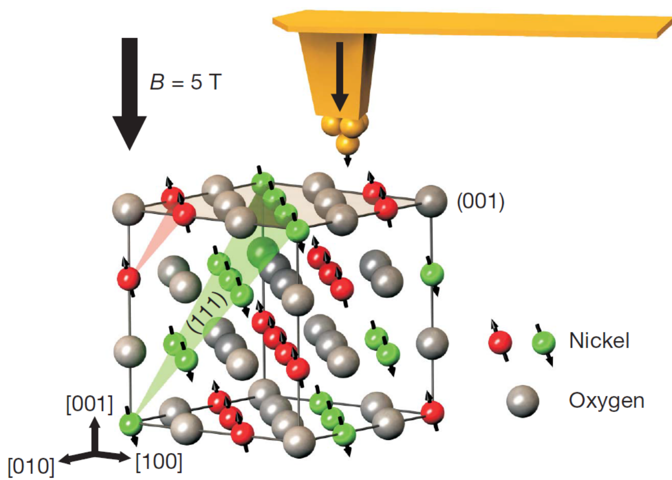

Figure 6. Antiferromagnetic preferences of NiO in the (001) plane shown. Iron coated silicon tip polarized parallel to the NiO(001) face with the help of a 5T magnetic field. Image from Kaiser et al[15].

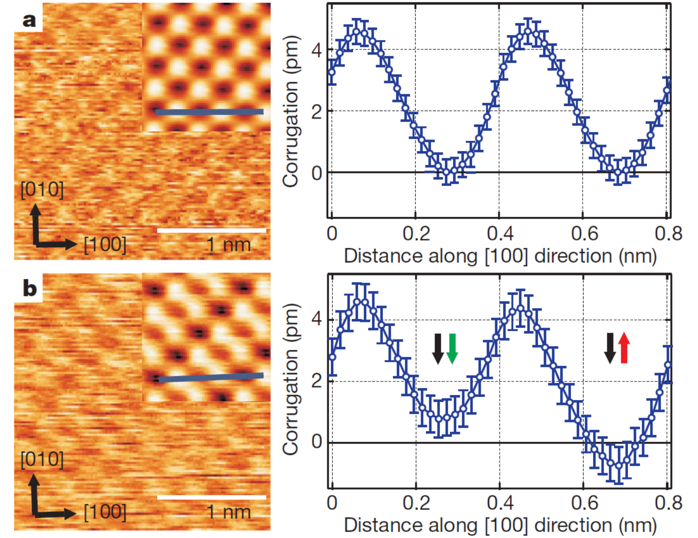

Figure 7. **(A)** AFM scan taken at $\Delta f = -22$ Hz. Here, the tip is to far away to have any noticeable spin-spin interactions. **(B)** AFM scan taken at $\Delta f = -23.4$ Hz, which brings the tip approximately 30 pm closer to the sample, making spin-spin interactions relevant. Image from Kaiser et al[15].

References

[1] G. Binnig, C. F. Quate, and C. Gerber, "Atomic force microscope," Phys. Rev. Lett. **56**, 930–933 (1986).

[2] Y. Seo and W. Jhe, "Atomic force microscopy and spectroscopy," Reports on Progress in Physics **71**, 016101 (2008).

[3] B. Voigtländer, *Scanning Probe Microscopy* (Springer, 2015).

[4] M. Guggisberg, M. Bammerlin, C. Loppacher, O. Pfeiffer, A. Abdurixit, V. Barwich, R. Bennewitz, A. Baratoff, E. Meyer, and H.-J. Güntherodt, "Separation of interactions by noncontact force microscopy," Phys. Rev. B **61**, 11151–11155 (2000).

[5] "Cypher - the world's highest resolution afm," `https://www.asylumresearch.com/Products/Cypher/Cypher.shtml`, accessed: 2016-11-11.

[6] F. J. Giessibl, "Atomic resolution of the silicon (111)-(7x7) surface by atomic force microscopy," Science **267**, 68–71 (1995).

[7] F. J. Giessibl, "Advances in atomic force microscopy," Rev. Mod. Phys. **75**, 949–983 (2003).

[8] L. Bartels *et al.*, "Dynamics of electron-induced manipulation of individual co molecules on cu(111)," Phys. Rev. Lett. **80**, 2004–2007 (1998).

[9] L. Gross *et al.*, "The chemical structure of a molecule resolved by atomic force microscopy," Science **325**, 1110–1114 (2009).

[10] M. A. Lantz *et al.*, "Quantitative measurement of short-range chemical bonding forces," Science **291**, 2580–2583 (2001).

[11] M. Abe, Y. Sugimoto, O. Custance, and S. Morita, "Room-temperature reproducible spatial force spectroscopy using atom-tracking technique," Applied Physics Letters **87**, 173503 (2005).

[12] R. Hoffmann, L. N. Kantorovich, A. Baratoff, H. J. Hug, and H. J. Güntherodt, "Sublattice identification in scanning force microscopy on alkali halide surfaces," Phys. Rev. Lett. **92**, 146103 (2004).

[13] Y. Sugimoto, P. Pou, M. Abe, P. Jelinek, R. Pérez, S. Morita, and Ó. Custance, "Chemical identification of individual surface atoms by atomic force microscopy," Nature **446**, 64–67 (2007).

[14] S. Heinze *et al.*, "Real-space imaging of two-dimensional antiferromagnetism on the atomic scale," Science **288**, 1805–1808 (2000).

[15] U. Kaiser, A. Schwarz, and R. Wiesendanger, "Magnetic exchange force microscopy with atomic resolution," Nature **446**, 522–525 (2007).